

PBGAN: Partial Binarization of Deconvolution Based Generators

Jinglan Liu
University of Notre Dame
jliu16@nd.edu

Jiaxin Zhang
University of Science and
Technology of China
zjx219@mail.ustc.edu.cn

Yukun Ding
University of Notre Dame
yding5@nd.edu

Xiaowei Xu
University of Notre Dame
xxu8@nd.edu

Meng Jiang
University of Notre Dame
mjiang2@nd.edu

Yiyu Shi
University of Notre Dame
yshi4@nd.edu

Abstract

The generator is quite different from the discriminator in a generative adversarial network (GAN). Compression techniques for the latter have been studied widely, while those for the former stay untouched so far. This work explores the binarization of the deconvolution based generator in a GAN for memory saving and speedup. We show that some layers of the generator may need to be kept in floating point representation to preserve performance, though conventional convolutional neural networks can be completely binarized. As such, only partial binarization may be possible for the generator. To quickly decide whether a layer can be binarized, supported by theoretical analysis and verified by experiments, a simple metric based on the dimension of deconvolution operations is established. Moreover, our results indicate that both generator and discriminator should be binarized at the same time for balanced competition and better performance. Compared with the floating-point version, experimental results based on CelebA suggest that our partial binarization on the generator of the deep convolutional generative adversarial network can yield up to $25.81\times$ saving in memory consumption, and $1.96\times$ and $1.32\times$ speedup in inference and training respectively with little performance loss measured by sliced Wasserstein distance.

1. Introduction

In recent years, generative adversarial networks (GANs), which are spin-offs from conventional convolutional neural networks (CNNs), have attracted much attention in the fields of reinforcement learning, unsupervised learning and also semi-supervised learning [11, 30, 35]. Some promising applications based on GANs include images reconstruc-

tion with super-resolution, art creation and image-to-image translation [12], many of which can run on portable devices. For example, one potential application of GAN allows videos to be broadcast in low resolution and then reconstructed to ultra-high resolution by end users [23] as shown in Figure 1.

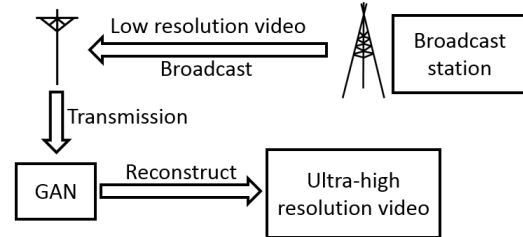


Figure 1. Low resolution broadcast based on GAN

However, the resources required by GANs to perform computations in real-time may not be easily accommodated by portable devices. For example, constructing an image of 64×64 resolution with deep convolutional generative adversarial network (DCGAN) [32] requires 86.6 MB of memory, most of which is used for the generator. The memory goes up to 620.8 MB for 1024×1024 resolution [21], and up to about 800 MB for the popular 4K video with resolution of 3840×2160 . On the other hand, one of the state-of-the-art mobile processors, A11 in the newest iPhone X [17], provides only 3 GB RAM, most of which must be occupied by the operating system and its peripherals. As a result, developers must restrict neural network models to just a few megabytes to avoid crash [6]. The memory budget gets even tighter when it comes to devices of smaller form factor such as Apple Watch series 3, which only has 786 MB RAM.

The same problem has been well known for conventional CNNs, and various solutions have been proposed via redesigning the algorithms and/or computation struc-

tures [14, 24, 40]. Among them, quantization until binary is one of the most popular techniques as it fits hardware implementation well with high efficiency [6, 16]. Its success on CNNs has been demonstrated by multiple works [15, 19, 42], where memory consumption is deeply compressed with almost preserved performance.

The same technique can be readily applied to discriminator networks in GANs, which are nothing different from conventional CNNs. It may be alluring to also apply it to binarize generators, especially the deconvolution [39] based ones as the computation process looks similar. However, instead of distilling local information from a global map as in convolution operations, deconvolution attempts to construct the global map by local information. This difference can lead to significantly different binarization results, as will be discussed in Section 3. Accordingly, a scheme tailored to deconvolution based generators is warranted.

In this paper, we show through theoretical analysis that under certain conditions, binarizing a deconvolution layer may cause significant performance loss. To quickly decide whether a layer can be binarized, supported by theoretical analysis and verified by experiments, a simple metric based on the dimension of deconvolution operations is established. We then propose the scheme of partial binarization of deconvolution based generators (PBGAN). Furthermore, we find that only binarizing the generator and leaving discriminator network unchanged will introduce unbalanced competition and performance degradation. Thus both networks should be binarized at the same time. Experimental results using DCGAN on CelebA suggest that PBGAN can yield up to $25.81\times$ saving in memory consumption, and $1.96\times$ and $1.32\times$ speedup in inference and training respectively with little performance loss measured by sliced Wasserstein distance (SWD).

2. Related works and background

2.1. CNN compression

Compression techniques for CNNs mainly consist of pruning, quantization, re-structure and other approximations based on mathematical matrix manipulations [14, 18, 25]. The main idea of the pruning method in [15] is to “prune” connections with smaller weights out so that both synapses and neurons are possible to be removed from the original structure. This can work well with traditional CNNs and reduce the number of parameters of AlexNet by a factor of nine [15]. Re-structure methods modify network structures for compression, such as changing functions or block order in layers [25, 33].

In this work, we focus on the quantization technique. Quantization aims to use fewer bits to present values of weights or even inputs. Quantization has been used to accelerate CNNs in various works at different levels [20, 28]

including ternary quantization [24, 43] and iterative quantization [41], with only small accuracy loss. In [14], the authors proposed to determine weight sharing after a network is fully trained, so that the shared weights approximate the original network. From a fully trained model, weights are clustered and replaced by the centroids of clusters. During retraining, the summation of the gradients in same groups are used for the fine-tuning of the centroids. Through such quantization, it is reported to be able to compress AlexNet up by around 8% before significant accuracy loss occurs.

A number of recent works [4, 8, 9, 16, 33, 42] pushed it further by using binarization to compress CNNs, where only a single bit is used to represent values. Training networks with weights and activations constrained to ± 1 was firstly proposed in [8]. Through transforming 32-bit floating point weight values to binary representation, CNNs with binary weights and activations are about $32\times$ smaller. In addition, when weight values are binary, convolutions can be estimated by only addition and subtraction without multiplication, which can achieve around $2.0\times$ speedup. However, the method introduces significant performance loss. To alleviate the problem, [33] proposed Binary-Weight-Network, where all weight values are binarized with an additional continuous scaling factor for each output channel. We will base our discussion on this weight binarization.

However, none of the existing works explored the compression of generators in GANs, where deconvolution replaces convolution as the major operation. Note that while there is a recent work that uses the term of “binary generative adversarial networks” [36], it is not about the binarization of GANs. In that work, only the inputs of the generator are restricted to binary code to meet the specific application requirement. All parameters inside the networks and the training images are not quantized.

2.2. GAN

GAN was developed by [13] as a framework to train a generative model by an adversarial process. In a GAN, a discriminative network (discriminator) learns to distinguish whether a given instance is real or fake, and a generator network (generator) learns to generate realistic instances to confuse the discriminator.

Originally, the discriminator and the generator of a GAN are both multilayer perceptrons. Researchers have since proposed many variants of it. For example, DCGAN transformed multilayer perceptrons to deep convolutional networks for better performance. Specifically, the generator is composed by four deconvolutional layers. GANs with such a convolutional/deconvolutional structure have also been successfully used to synthesize plausible visual interpretations of given text [34] and to learn interpretable and disentangled representation from images in an unsupervised way [7]. Wasserstein generative adversarial networks (WGAN)

[2] and least squares generative adversarial networks (LS-GAN) [27] have been proposed with different loss functions to achieve more stable performance, yet they both employed the deconvolution operations too.

3. Analysis on power of representation

In this section, we analyze the power of a deconvolution layer to represent any given mapping between the input and the output, and how such power will affect the performance after binarization. We will show that the performance loss of a layer is related to the dimension of the deconvolution, and develop a metric called the degree of redundancy to indicate the loss. Finally, based on the analysis, several inferences are deduced at the end of this section.

In the discussion below, we ignore batch normalization as well as activation operations and focus on the deconvolution operation in a layer, as only the weights in that operation are binarized. The deconvolution process can be transformed to equivalent matrix multiplication. Let $\mathbf{D}^I \in \mathcal{R}^{c_i \times h_i \times w_i}$, where c_i , h_i and w_i are number of channels, height and width of the input respectively) be the input matrix, and $\mathbf{D}^O \in \mathcal{R}^{c_o \times h_o \times w_o}$, where c_o , h_o and w_o are the number of channels, height and width of the output respectively) be the output matrix. Denote $\mathbf{K} \in \mathcal{R}^{c_i \times c_o \times h_k \times w_k}$, where h_k and w_k are the height and width of a kernel in the weight matrix) as the weight matrix to be deconvoluted with \mathbf{D}^I . Padding is ignored in the discussion, since it will not effect the results.

For the deconvolution operation, the local regions in the output can be stretched out into columns, by which we can cast \mathbf{D}^O to $\mathbf{D}^{Od} \in \mathcal{R}^{s_i \times r_o}$, where $s_i = h_i w_i$, $r_o = c_o h_k w_k$. Similarly, $\mathbf{D}^{Id} \in \mathcal{R}^{s_i \times c_i}$ can be restructured from \mathbf{D}^I , and $\mathbf{K}^d \in \mathcal{R}^{c_i \times r_o}$ can be restructured from \mathbf{K} , where $s_i = h_i w_i$, $r_o = c_o h_k w_k$. Please refer to [10] for details about the transform. Then, the deconvolution operation can be compactly written as

$$\mathbf{D}^{Od} = \mathbf{D}^{Id} * \mathbf{K}^d, \quad (1)$$

where $*$ denotes matrix multiplication. \mathbf{D}^{Id} and \mathbf{D}^{Od} are the matrices containing pixels for an image or an intermediate feature map. During the training process, we adjust the values of \mathbf{K}^d to construct a desired mapping between \mathbf{D}^{Id} and \mathbf{D}^{Od} .

We use $(\cdot)_j$ to denote the j -th column of a matrix. Then (1) can be decomposed column-wise as

$$\mathbf{D}_j^{Od} = \mathbf{D}^{Id} * \mathbf{K}_j^d, 1 \leq j \leq r_o, \quad (2)$$

where $\mathbf{K}_j^d \in \mathcal{R}^{c_i}$ and $\mathbf{D}_j^{Od} \in \mathcal{R}^{s_i}$.

Now we analyze a mapping between an arbitrary input \mathbf{D}^{Id} and an arbitrary output \mathbf{D}_j^{Od} . From (2), when the weights are continuously selected, all vectors that can be

expressed by the right hand expression is a subspace Ω spanned by the columns of \mathbf{D}^{Id} , the dimension of which is c_i . Here we have assumed without loss of generality that \mathbf{D}^{Id} has full column rank. When $c_i < s_i$, which is the dimension of the output space Φ where \mathbf{D}_j^{Od} lies, Ω is of lower dimension than Φ , and accordingly, \mathbf{D}_j^{Od} can either be uniquely expressed as a linear combination of the columns in \mathbf{D}^{Id} if it lies in Ω (e.g. a unique \mathbf{K}_j^d exists), or cannot be expressed if it is not (e.g. no such \mathbf{K}_j^d exists). When $c_i = s_i$, Ω and Φ are equivalent, and any \mathbf{D}_j^{Od} can be uniquely expressed as a linear combination of the columns in \mathbf{D}^{Id} . When $c_i > s_i$, Ω and Φ are still equivalent, but any \mathbf{D}_j^{Od} can be expressed as an infinite number of different linear combinations of the columns in \mathbf{D}^{Id} . In fact, the coefficients \mathbf{K}_j^d of these combinations lie in a $(c_i - s_i)$ -dimensional sub-space Ψ .

The binarization imposes a constraint on the possible values of the elements in \mathbf{K}_j^d . Only finite number of combinations are possible. If $c_i \leq s_i$, then at least one of these combinations has to be proportional to the unique \mathbf{K}_j^d that yields the desired \mathbf{D}_j^{Od} to preserve performance. If $c_i > s_i$, then one of these combinations needs to lie in the subspace Ψ to preserve performance. Apparently, the larger the dimension of Ψ is, the more likely this will happen, and the less the performance loss is. A detailed math analysis is straightforward to illustrate this, and is omitted here in the interest of space. Accordingly, we define the dimension of Ψ , $c_i - s_i$, as the degree of redundancy in the rest of the paper. Note that when this metric is negative, it reflects that Ω is of lower dimension than Φ and thus this deconvolution layer is more vulnerable to binarization errors. In general, a higher degree of redundancy should give lower binarization error.

We will use a small numerical example to partially validate the above discussion. We construct a deconvolution layer and vary its degree of redundancy by adjusting the input size. For each degree of redundancy we calculate the minimum average Euclidean distance to the same given vector after the weights are binarized, which reflects the error introduced through the binarization process. The minimum average Euclidean distance is obtained by enumerating all the possible combinations of the weights. The results are depicted in Figure 2. From the figure we can see that the error decreases with the increase of degree of redundancy, which matches our discussion.

For generators in most state-of-the-art GAN models [27, 32], we find that the degree of redundancy reduces with the increase in depth, eventually dropping below zero. For example, for the generator of DCGAN presented in [32], the degree of redundancy v.s. depth is plotted in Figure 3. The degree of redundancy of the last layer drops to -896. Such a decrease reflects the fact that more details are generated at the output of a layer as its depth grows, as can also be seen

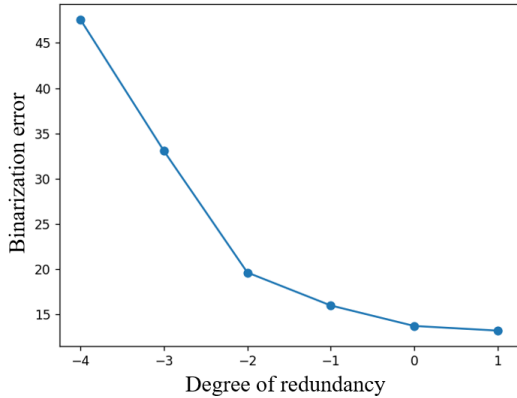


Figure 2. Binarization error v.s. degree of redundancy for a deconvolution layer.

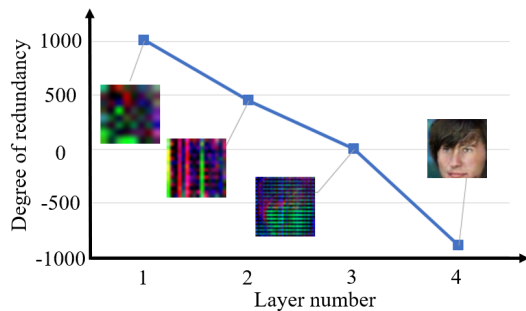


Figure 3. Degree of redundancy v.s. layer number for DCGAN. The intermediate feature maps at the output of each layer as well as the final output are also presented.

in Figure 3. These details are highly correlated, and reduce the subspace needed to cover them. Therefore, several inferences can be deduced:

- The last one or a few layers with negative degree of redundancy should be kept un-binarized to avoid excessive performance loss.
- Since the degree of redundancy decreases as the depth increases, binarizing shallower layers will lead to lower performance loss.
- Whether a layer can be binarized without large performance loss does not depend on other layers. Accordingly, the binarizability of a layer can be superposed. If a layer can be binarized alone, it can be binarized with other such layers.
- When binarizing several deconvolution layers together, the layer with the least degree of redundancy may be the bottleneck of the generator’s performance.

4. Experimental setup

4.1. DCGAN and its different binarization settings

DCGAN will serve as a vehicle to verify the inferences deduced from the theoretical analysis in Section 3. We will explore how to best binarize it with preserved performance. Specifically, we use the TensorFlow [1] implementation of DCGAN on GitHub [22]. The structure of its generator is illustrated in Figure 4. The computed degree of redundancy in each layer in the generator is shown in Figure 3 and qualitatively summarized in Table 1.

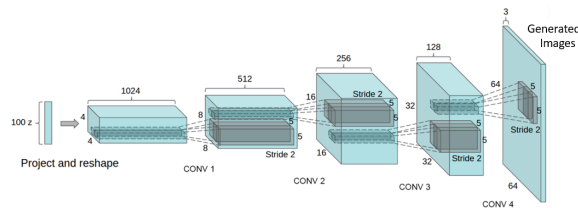


Figure 4. Structure of the generators in DCGAN with dimension of each layer labeled (figure credit: [32])

Table 1. Degree of redundancy in each deconvolution layer of the generator in DCGAN

Layer number	Degree of redundancy
1	1008
2	448
3	0
4	-896

To verify inferences deduced in the Section 3, we will discuss a total of eight different settings to binarize the generator of DCGAN, which are summarized in Table 2 for clarity. In this table, the “Setting” column labels each setting. “Layer(s) binarized” indicates which layer(s) are binarized in the generator. Since there are four deconvolution layers in total in the generator, available numbers are from one to four. The “Discriminator binarized” column tells whether the discriminator is binarized or not. “Y” means yes, while “N” means no. This column is introduced to verify an observation in our experiments to be discussed later.

Setting G works as the performance baseline, because it adopts the existing binarization strategy directly[33]. The degree of redundancy is not taken into consideration during the binarization process in Setting G.

4.2. Dataset and metrics

CelebA [26] is used as the dataset for our experiments, because it is a popular and verified dataset for different GAN structures. DCGAN, WGAN, LSGAN and many other GAN structures are tested on it [5]. As every image in

Table 2. Settings of different partial binarization of generator in DCGAN

Setting	Layer(s) binarized	Discriminator binarized
A	None	N
B	1	N
C	2	N
D	3	N
E	4	N
F	1,2,3	N
G	1,2,3,4	N
H	1,2,3	Y

CelebA contains only one face, it is much easier to tell the quality of the generated images.

Traditionally the quality of the generated images is identified by observation. However, qualitatively evaluation is always a hard problem. According to the in-depth analysis of commonly used criteria in [37], good performance in a single or extrapolated metric from average log-likelihood, Parzen window estimates, and visual fidelity of samples does not directly translate to good performance of a GAN. On the other hand, the log-likelihood score proposed in [38] only estimates a lower bound instead of the actual performance.

Very recently, [21] proposed an efficient metric, which we will use in our experiments, and showed that it is superior to MS-SSIM [29]. It calculates the sliced Wasserstein distance (SWD) between the training samples and the generated images under different resolutions up to the maximum that both the training samples and the generated images can achieve. In this work, the max resolution is 64×64 .

Specifically, SWD evaluates the quality of the generated images by considering the multi-scale statistical similarity between distributions of patches drawn via Laplacian pyramid [3] from training samples and generated images, starting at the resolution of 16×16 pixels [21]. The pyramid progressively doubles, each successive resolution encoding the difference between the training samples and generated ones to an up-sampled version of the previous one. A single Laplacian pyramid level corresponds to a specific spatial frequency band. A total of 16,384 images are randomly selected and 128 descriptors from each resolution in the Laplacian pyramid are extracted in [21]. Each descriptor is a 7×7 pixel neighborhood with three channels from each image, which is denoted as $\mathbf{x} \in \mathcal{R}^{7 \cdot 7 \cdot 3} = \mathcal{R}^{147}$. Patches from resolution level l of the training samples and generated images are denoted as $\{\mathbf{x}_i^l\}$ and $\{\mathbf{y}_i^l\}$ ($1 \leq i \leq 16384 \cdot 128$), respectively. $\{\mathbf{x}_i^l\}$ and $\{\mathbf{y}_i^l\}$ are normalized with respect to the mean and standard deviation of each channel at first, and then the statistical similarity is estimated by computing the sliced Wasserstein distance between them, which is ef-

ficiently computable [31]. The same experimental settings as in [21] are followed in our experiments.

For all different resolutions, small SWD indicates that the distributions of the patches are similar, which means that a generator with smaller SWD is expected to produce images more similar to the images from the training samples in both appearance and variation. In particular, the SWD from the lower resolution patches indicates similarity in holistic image structures, while the finer-level patches encode information about pixel-level attributes [21].

5. Experimental results

In this section, we will present experimental results that verify our inferences in Section 3, along with some additional observations about the competition between the generator and the discriminator. The images generated by the original GAN (setting A), in which all weights of each deconvolution layer are in the form of floating point, are displayed in Figure 5(a).

5.1. Qualitative comparison of single-layer binarization

We start our experiments by comparing the images generated by binarizing a single layer in the generator of DCGAN and the results are shown in Figures 5(b) - 5(e), which are generated by PBGAN under setting B - setting E respectively. In other words, those PBGANs utilize binary weights to the first, second, third and the last deconvolution layer respectively. The degree of redundancy of each layer is shown in Figure 3. From the generated figures we can then see that Figure 5(b) generates the highest quality of images, similar to the original ones in Figure 5(a). Images in Figure 5(c) are slightly inferior to those in Figure 5(b), but better than those in Figure 5(d). Figure 5(e) has no meaningful images at all. These observations are in accordance with our inferences in Section 3: the performance loss when binarizing a layer is decided by its degree of redundancy, and a layer with negative degree of redundancy should not be binarized.

5.2. Quantitative comparison of single-layer binarization

We further quantitatively compute the SWD values with 16×16 , 32×32 and 64×64 resolutions for the four different settings B, C, D, and E. Their relationship with the degree of redundancy is plotted in Figure 6. From the figure, two things are clear: first, regardless of resolution, a negative degree of redundancy (setting E) results in a more than $5 \times$ increase in SWD compared with other settings with positive degree of redundancy (settings B, C, and D). Second, for all the three resolutions, SWD decreases almost linearly with the increase of the degree of redundancy when it is positive. This confirms that our degree of redundancy can capture the impact of binarization not only on the holistic structure but



Figure 5. Images generated under different settings

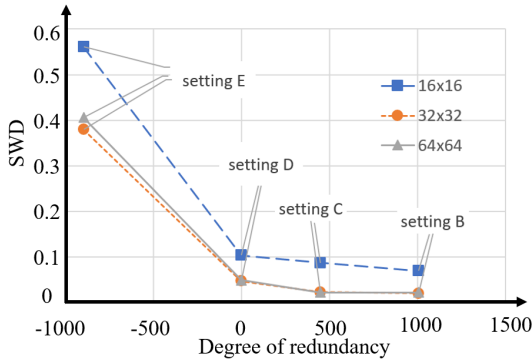


Figure 6. SWD v.s. degree of redundancy in different settings

also on the pixel-level fine details, and as such, is indeed a good indicator to quickly judge whether a layer can be binarized.

Table 3. Average SWD under different settings

Setting	A	B	C	D	E
Average SWD ($\times 10^{-3}$)	44	38	45	67	449

We also report the SWD averaged over different resolutions (16x16, 32x32, 64x64) in Table 3, where the result for the original GAN (setting A) is also reported. From the table we can draw similar conclusions, that binarizing second layer (setting C) increases the average SWD by 18.4% compared with binarizing the first layer (setting B), while

binarizing third and fourth layer (settings D and E) further increases it by 76.3% and 1081.6%, respectively.

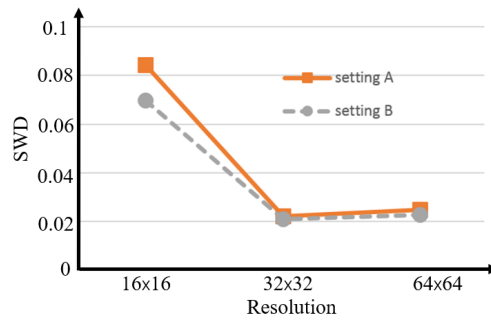


Figure 7. SWD v.s. resolution under setting A and setting B

It is interesting to note that the average SWD achieved by binarizing the first layer (setting B) is 13.6% smaller than that by the original DCGAN (setting A). To further check this, we plot the SWD v.s. resolution for these two settings in Figure 7. From the figure we can see that the SWD from setting B is always smaller than that from setting A across all three resolutions. This shows that setting B can achieve better similarity as well as detailed attributes. Such an improvement is probably due to the regularization effect, and similar effect has been observed in the compression of CNNs [4].

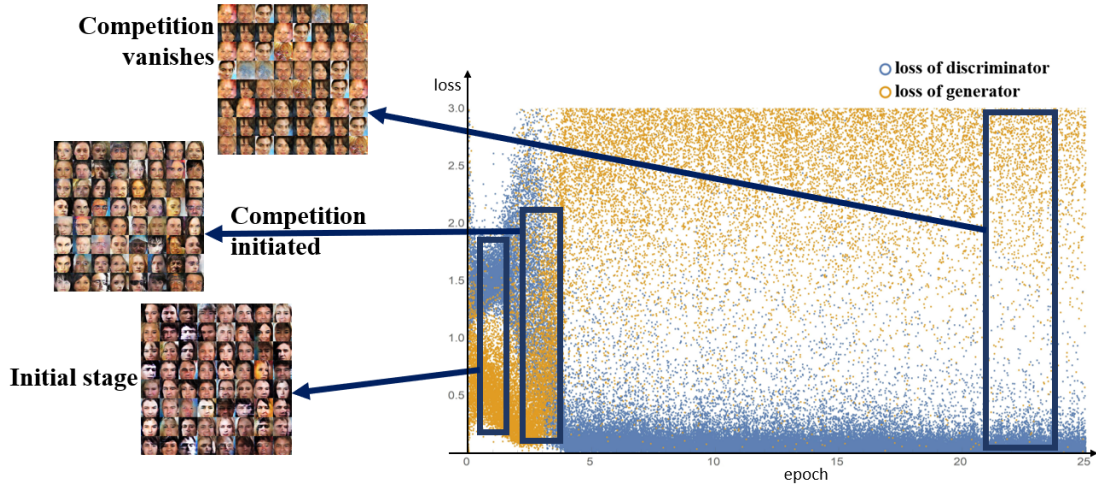


Figure 8. Loss values of PBGAN under setting F along epochs

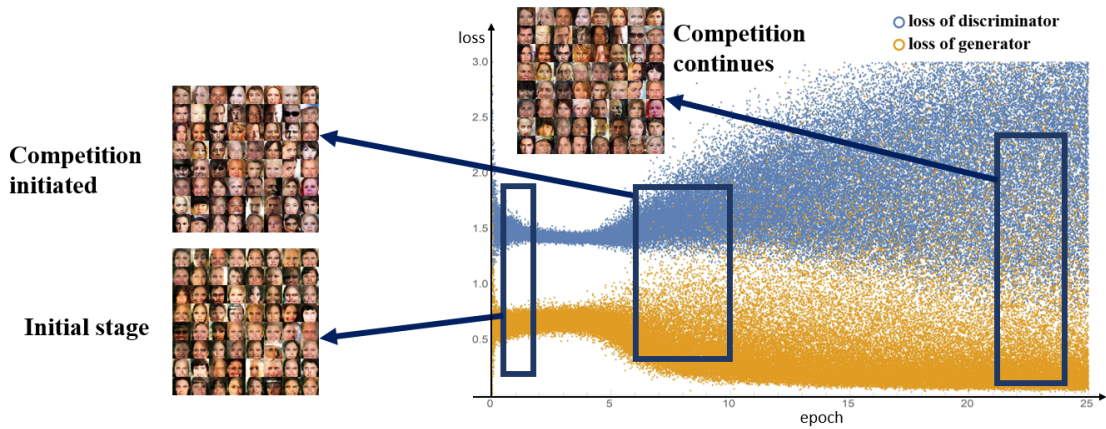


Figure 9. Loss values of PBGAN under setting H along epochs

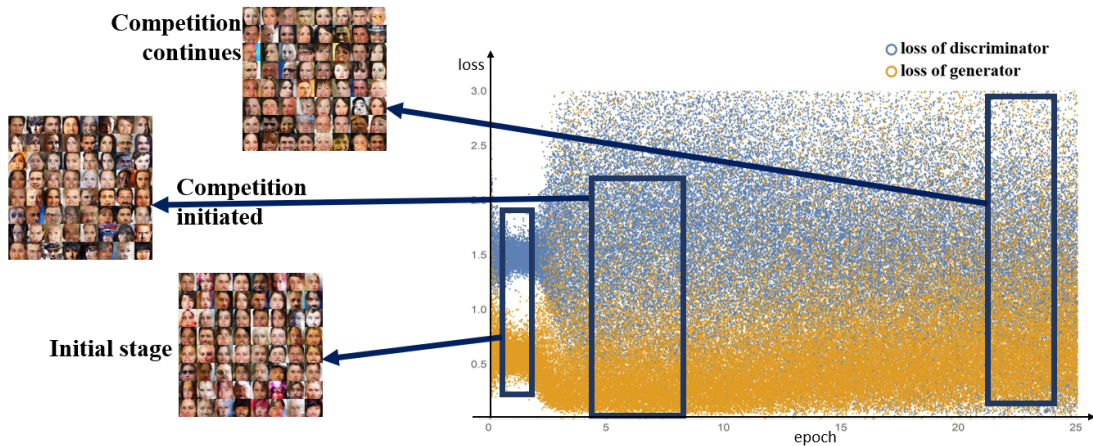


Figure 10. Loss values of PBGAN under setting A along epochs

5.3. Validation of superposition of binarizability

We now explore experiments to verify our inference that all layers that can be binarized along can be binarized to-

gether. The images generated by setting F in Figure 5(f), where the first three layers in the generator are binarized together, show no significant difference from those in Figures

5(a)- 5(d). On the other hand, setting G does not generate any meaningful output (Figure 5(g)), as the last layer, which cannot be binarized alone, is binarized together with the first three layers. This qualitatively confirms the inference.

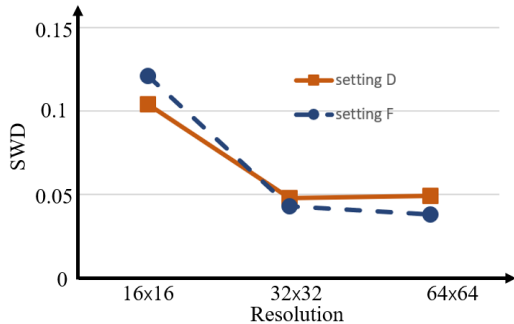


Figure 11. SWD v.s. resolutions under setting D and setting F

The average SWD for setting F is 0.067, the same as setting D. Further looking at the SWD values under different resolutions for the two different settings as shown in Figure 11, it is clear that the two curves are very close. This validates our last inference, that when multiple layers are binarized together, the layer with least degree of redundancy is the bottleneck, which decides the overall performance of the network.

5.4. Compression Saving

Table 4 summarizes the average speedup during training and inference as well as the memory reduction for PBGAN compared with the original generator in DCGAN. PBGAN under setting F can achieve $25.81 \times$ memory saving as well as $1.96 \times$ and $1.32 \times$ speedup during inference and training respectively. For both DCGAN and PBGAN, during the training process the floating point representation of all weights need to be used for backward propagation and update. As such, the speedup mainly comes from faster forward propagation with binarized weights. This is why the speedup for training is much less compared with that for inference. Compression savings are also shown in Table 4.

Table 4. Training and inference speedup as well as memory reduction for PBGAN

Generator model	Speedup		Memory cost
	Inference	Training	
DCGAN (setting A)	1.0 \times	1.0 \times	1.0 \times
PBGAN (setting F)	1.96 \times	1.32 \times	1/25.81 \times

5.5. Unbalanced competition

So far our discussion has focused on the binarization of the generator in a GAN only, as the discriminator takes the

same form as conventional CNNs. However, since competition between generator and discriminator is the key of GANs, would a binarized generator still compete well with a full discriminator?

The loss values for the discriminator network and the generator of PBGAN under setting F are depicted in Figure 8, where x-axis indicates the number of epochs and y-axis is the loss value. The images generated from different number of epochs are also exhibited aside. From the figure we can see that during the initial stage, distorted faces are generated. As the competition is initiated, image quality improves. But very quickly, the competition vanishes and the generated images stop improving. However, when we binarize the discriminator at the same time (setting H), the competition continues to improve, as can be seen in Figure 9. We further plot the loss values of the discriminator and the generator of the original DCGAN (setting A), and the results are shown in Figure 10. It is very similar to Figure 9, except that the competition is initiated earlier, which is due to the stronger representation power of both the generator and the discriminator before binarization. These figures confirm that the quick disappearance of competition is mainly due to the unbalanced generator and discriminator, which should be avoided.

We now explore the quality of the images generated from balanced competition, *e.g.* using setting H. The images generated are shown in Figure 5(h), the quality of which is apparently better than the rest in Figures 5. To further confirm this quantitatively, we compute the average SWD values of those images, which is 0.034 in average. This is smaller than any average SWD values listed in Table 3, which shows that the images are of better quality, even compared with the original GAN.

5.6. Summary

To summarize the discussion and comparisons in this section, we plot the SWD v.s. resolution curves for all the 8 settings in Figures 12. It allows a complete view of how these different settings compare in terms of similarity as a whole and fine details. From the figure we can see that setting H gives the best similarity as a whole, while setting C yields the finest detailed attributes.

6. Conclusion

This paper explores the binarization of deconvolution based generators for memory reduction and speedup. We show that unlike convolutional neural networks, the generator cannot be fully binarized without significant performance loss. Through theoretical analysis, a degree of redundancy metric is proposed based on the dimension of deconvolution operation, which provides a fast indication whether a layer can be binarized or not. We also demonstrate that both generator and discriminator should be bina-

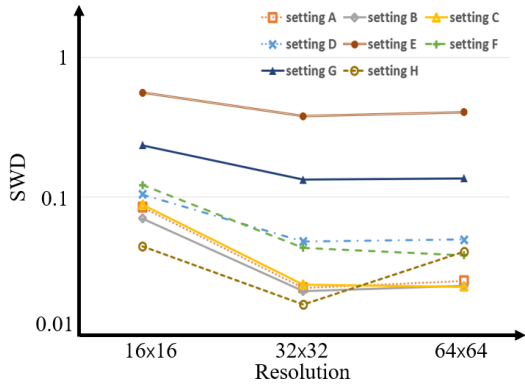


Figure 12. SWD v.s. resolutions under all different settings

rized at the same time for a balanced competition and better performance. Experimental results based on CelebA suggest that our partial binarization on DCGAN can yield up to $25.81\times$ saving in memory consumption with $1.96\times$ and $1.32\times$ speedup in inference and training respectively with little performance loss measured by sliced Wasserstein distance score.

References

- [1] M. Abadi, A. Agarwal, P. Barham, E. Brevdo, Z. Chen, C. Citro, G. S. Corrado, A. Davis, J. Dean, M. Devin, et al. Tensorflow: Large-scale machine learning on heterogeneous distributed systems. *arXiv preprint arXiv:1603.04467*, 2016. 4
- [2] M. Arjovsky, S. Chintala, and L. Bottou. Wasserstein generative adversarial networks. In *International Conference on Machine Learning*, pages 214–223, 2017. 3
- [3] P. J. Burt and E. H. Adelson. Readings in computer vision: Issues, problems, principles, and paradigms. chapter the laplacian pyramid as a compact image code. *Morgan Kaufmann Publishers Inc., San Francisco, CA, USA*, pages 671–679, 1987. 5
- [4] Z. Cai, X. He, J. Sun, and N. Vasconcelos. Deep learning with low precision by half-wave gaussian quantization. *arXiv preprint arXiv:1702.00953*, 2017. 2, 6
- [5] J. Cha. tf.gans-comparison, 2017. 4
- [6] W. Chen, J. Wilson, S. Tyree, K. Weinberger, and Y. Chen. Compressing neural networks with the hashing trick. In *International Conference on Machine Learning*, pages 2285–2294, 2015. 1, 2
- [7] X. Chen, Y. Duan, R. Houthoofd, J. Schulman, I. Sutskever, and P. Abbeel. Infogan: Interpretable representation learning by information maximizing generative adversarial nets. In *Advances in Neural Information Processing Systems*, pages 2172–2180, 2016. 2
- [8] M. Courbariaux, Y. Bengio, and J.-P. David. Binaryconnect: Training deep neural networks with binary weights during propagations. In *Advances in Neural Information Processing Systems*, pages 3123–3131, 2015. 2
- [9] M. Courbariaux, I. Hubara, D. Soudry, R. El-Yaniv, and Y. Bengio. Binarized neural networks: Training deep neural networks with weights and activations constrained to+ 1 or-1. *arXiv preprint arXiv:1602.02830*, 2016. 2
- [10] cs231n Course Materials. Implementation as Matrix Multiplication, 2017. 3
- [11] C. Finn, I. Goodfellow, and S. Levine. Unsupervised learning for physical interaction through video prediction. In *Advances in Neural Information Processing Systems*, pages 64–72, 2016. 1
- [12] I. Goodfellow. Nips 2016 tutorial: Generative adversarial networks. *arXiv preprint arXiv:1701.00160*, 2016. 1
- [13] I. Goodfellow, J. Pouget-Abadie, M. Mirza, B. Xu, D. Warde-Farley, S. Ozair, A. Courville, and Y. Bengio. Generative adversarial nets. In *Advances in neural information processing systems*, pages 2672–2680, 2014. 2
- [14] S. Han, H. Mao, and W. J. Dally. Deep compression: Compressing deep neural networks with pruning, trained quantization and huffman coding. *arXiv preprint arXiv:1510.00149*, 2015. 2
- [15] S. Han, J. Pool, J. Tran, and W. Dally. Learning both weights and connections for efficient neural network. In *Advances in Neural Information Processing Systems*, pages 1135–1143, 2015. 2
- [16] I. Hubara, M. Courbariaux, D. Soudry, R. El-Yaniv, and Y. Bengio. Quantized neural networks: Training neural networks with low precision weights and activations. *arXiv preprint arXiv:1609.07061*, 2016. 2
- [17] A. Inc. Apple Inc., 2017. 1
- [18] M. Jaderberg, A. Vedaldi, and A. Zisserman. Speeding up convolutional neural networks with low rank expansions. *arXiv preprint arXiv:1405.3866*, 2014. 2
- [19] N. P. Jouppi, C. Young, N. Patil, D. Patterson, G. Agrawal, R. Bajwa, S. Bates, S. Bhatia, N. Boden, A. Borchers, et al. In-datacenter performance analysis of a tensor processing unit. *arXiv preprint arXiv:1704.04760*, 2017. 2
- [20] P. Judd, J. Albericio, T. Hetherington, T. M. Aamodt, and A. Moshovos. Stripes: Bit-serial deep neural network computing. In *Microarchitecture (MICRO), 2016 49th Annual IEEE/ACM International Symposium on*, pages 1–12. IEEE, 2016. 2
- [21] T. Karras, T. Aila, S. Laine, and J. Lehtinen. Progressive growing of gans for improved quality, stability, and variation. *arXiv preprint arXiv:1710.10196*, 2017. 1, 5
- [22] T. Kim. DCGAN-tensorflow, 2017. 4
- [23] C. Ledig, L. Theis, F. Huszár, J. Caballero, A. Cunningham, A. Acosta, A. Aitken, A. Tejani, J. Totz, Z. Wang, et al. Photo-realistic single image super-resolution using a generative adversarial network. *arXiv preprint arXiv:1609.04802*, 2016. 1
- [24] F. Li, B. Zhang, and B. Liu. Ternary weight networks. *arXiv preprint arXiv:1605.04711*, 2016. 2
- [25] M. Lin, Q. Chen, and S. Yan. Network in network. *arXiv preprint arXiv:1312.4400*, 2013. 2
- [26] Z. Liu, P. Luo, X. Wang, and X. Tang. Deep learning face attributes in the wild. In *Proceedings of International Conference on Computer Vision (ICCV)*, 2015. 4

- [27] X. Mao, Q. Li, H. Xie, R. Y. Lau, Z. Wang, and S. P. Smolley. Least squares generative adversarial networks. *arXiv preprint ArXiv:1611.04076*, 2016. 3
- [28] D. Miyashita, E. H. Lee, and B. Murmann. Convolutional neural networks using logarithmic data representation. *arXiv preprint arXiv:1603.01025*, 2016. 2
- [29] A. Odena, C. Olah, and J. Shlens. Conditional image synthesis with auxiliary classifier gans. *arXiv preprint arXiv:1610.09585*, 2016. 5
- [30] D. Pfau and O. Vinyals. Connecting generative adversarial networks and actor-critic methods. *arXiv preprint arXiv:1610.01945*, 2016. 1
- [31] J. Rabin, G. Peyré, J. Delon, and M. Berton. Wasserstein barycenter and its application to texture mixing. In *International Conference on Scale Space and Variational Methods in Computer Vision*, pages 435–446. Springer, 2011. 5
- [32] A. Radford, L. Metz, and S. Chintala. Unsupervised representation learning with deep convolutional generative adversarial networks. *arXiv preprint arXiv:1511.06434*, 2015. 1, 3, 4
- [33] M. Rastegari, V. Ordonez, J. Redmon, and A. Farhadi. Xnornet: Imagenet classification using binary convolutional neural networks. In *European Conference on Computer Vision*, pages 525–542. Springer, 2016. 2, 4
- [34] S. Reed, Z. Akata, X. Yan, L. Logeswaran, B. Schiele, and H. Lee. Generative adversarial text to image synthesis. *arXiv preprint arXiv:1605.05396*, 2016. 2
- [35] T. Salimans, I. Goodfellow, W. Zaremba, V. Cheung, A. Radford, and X. Chen. Improved techniques for training gans. In *Advances in Neural Information Processing Systems*, pages 2234–2242, 2016. 1
- [36] J. Song. Binary generative adversarial networks for image retrieval. *arXiv preprint arXiv:1708.04150*, 2017. 2
- [37] L. Theis, A. van den Oord, and M. Bethge. A note on the evaluation of generative models. *stat*, 1050:24, 2016. 5
- [38] Y. Wu, Y. Burda, R. Salakhutdinov, and R. Grosse. On the quantitative analysis of decoder-based generative models. *arXiv preprint arXiv:1611.04273*, 2016. 5
- [39] M. D. Zeiler, D. Krishnan, G. W. Taylor, and R. Fergus. Deconvolutional networks. In *Computer Vision and Pattern Recognition (CVPR), 2010 IEEE Conference on*, pages 2528–2535. IEEE, 2010. 2
- [40] S. Zhang, Z. Du, L. Zhang, H. Lan, S. Liu, L. Li, Q. Guo, T. Chen, and Y. Chen. Cambricon-x: An accelerator for sparse neural networks. In *Microarchitecture (MICRO), 2016 49th Annual IEEE/ACM International Symposium on*, pages 1–12. IEEE, 2016. 2
- [41] A. Zhou, A. Yao, Y. Guo, L. Xu, and Y. Chen. Incremental network quantization: Towards lossless cnns with low-precision weights. *arXiv preprint arXiv:1702.03044*, 2017. 2
- [42] S. Zhou, Y. Wu, Z. Ni, X. Zhou, H. Wen, and Y. Zou. Dorefa-net: Training low bitwidth convolutional neural networks with low bitwidth gradients. *arXiv preprint arXiv:1606.06160*, 2016. 2
- [43] C. Zhu, S. Han, H. Mao, and W. J. Dally. Trained ternary quantization. *arXiv preprint arXiv:1612.01064*, 2016. 2